A ^{129}Xe NMR Study of Functionalized Ordered Mesoporous Silica

Igor L. Moudrakovski,* Victor V. Terskikh, Christopher I. Ratcliffe, and John A. Ripmeester

Steacie Institute for Molecular Sciences, National Research Council, Ottawa, Ontario, Canada K1A 0R6

Li-Qiong Wang,* Yongsoon Shin, and Gregory J. Exarhos

Material Science Department, Pacific Northwest National Laboratory, Richland, Washington 99352

Received: December 18, 2001; In Final Form: April 3, 2002

In this publication we report the first application of continuous flow hyperpolarized (HP) ^{129}Xe techniques to studies of pore structure in ordered mesoporous materials. In particular, we report extensive ^{129}Xe NMR chemical shift measurements of xenon adsorbed in mesoporous materials of different porosities and surface chemical composition. The use of HP Xe has allowed us to work at very low concentrations of xenon where the contribution of the Xe−Xe interactions is negligible and the observed ^{129}Xe chemical shift reflects mainly interactions between the xenon atoms and the surface. Variable temperature measurements gave access to information on the adsorption parameters of xenon, and allowed us to follow the changes in these properties due to modification of the mesopore voids. Our ^{129}Xe NMR data reveal a nonuniform porosity and irregular pore structure in contrast to N_2 adsorption and TEM measurements that indicate regular nanoporous channels.

Introduction

Mesoporous silicate materials consisting of an ordered network of nanometer size channels were first introduced by Mobil researchers in the early 1990s.[1,2] After a decade of intensive study, these materials still generate strong interest because of their unique properties. The large size of the pores, which can vary from one to tens of nanometers, promotes enhanced diffusion properties. Combined with an extremely high internal surface area, their use is mandated in catalysis applications.[3,4] Such materials also have potential use in advanced separation methods and chromatography.[5] During the past decade, many mesoporous materials with different chemical compositions have been prepared. These include alumina, zirconia, titania, niobia, manganese oxide, and others.[6,7] Silica-based materials, however, are still the most commonly used and studied, principally because of their structural and chemical reproducibility and relatively uncomplicated synthesis.

Most applications of these mesoporous materials usually require functionalization of a relatively inactive silica surface that forms the internal pore structure. Chemically active organic or inorganic centers can be integrated into the channels of these materials, enhancing their reactivity and thereby opening up numerous applications in chemistry and biology.[8] Several approaches can be used to incorporate organic functional groups and molecules into mesoporous materials (hereafter referred to as functionalization), mostly for catalytic applications.[4] One method for generating functional centers in mesoporous materials is through the postsynthesis attachment of desired molecular species to the walls of the mesoporous channels. This approach has led to the development of a class of hybrid nanoscale materials that has already demonstrated great potential for many applications, such as adsorption, ion exchange, catalysis, and sensing.[9−13] The assembly of molecular structures within mesopores also provides a tool for rational engineering of surface properties. For example, hybrid mesoporous materials that contain specific chemical sites show exceptional selectivity and capacity in the adsorption of heavy metal ions from contaminated waste streams.[9,10] Besides heavy metals, more efficient materials have also been developed for extracting anions such as chromate and arsenate,[11] and radionuclides.[13]

Methods for functionalizing mesoporous materials have been reviewed recently by Möller and Bein.[14] Functionalization through direct silanation depends on the population density of hydroxyl groups that exist on the surface.[15,16] The problem of low hydroxyl concentration can be partially solved by using noncalcined mesoporous silica prepared using a neutral surfactant, with the surfactant being subsequently removed by solvent-extraction techniques.[9] High-density organic molecular monolayers can be constructed by purposely introducing physically adsorbed layers of water molecules prior to silanation.[10] Alternatively, co-condensation is a one-step process in which functionality is incorporated into the materials during self-assembly in solution.[17]

In general, the surface properties of chemically modified porous hybrid materials can be tailored with respect to pore size and surface chemistry on a molecular scale. The properties of such hybrid porous materials are determined by channel size, pore structure regularity, connectivity of the pores, resident chemical functionality, and molecular conformation of the molecules bound to the surface. Thus, it is crucial to determine these key parameters in order to have better control of the surface properties at the molecular level.

Molecular ordering on flat surfaces and ordering resulting from van der Waals interactions have been studied extensively by atomic force microscopy (AFM), contact angle measurements, small angle scattering, and some other techniques.[18] Compared to flat substrates, the molecular structures in mesoporous silica are more complex because of the unique confined geometry of the mesopore void space. Fortunately, the high surface area makes it possible to use molecular spectroscopic techniques such as nuclear magnetic resonance (NMR) to study molecular attachment and ordering within the mesopores.

* Authors to whom correspondence should be addressed.

10.1021/jp014585a CCC: $22.00
Published on Web 05/18/2002

Solid-state ^{13}C and ^{29}Si NMR techniques have been used to study the chain conformation and mobility of molecular layers in mesoporous silica.[12,19] Since the pore diameter and the regularity of the pore structure have large implications on how molecules are arranged in these pore channels, it is difficult to obtain a clear picture of bound molecular layers on pore surfaces using ^{13}C and ^{29}Si NMR alone. Although pore size, pore volume, and surface area are, in principle, accessible from X-ray powder diffraction, transmission electron microscopy, and nitrogen sorption measurements, the connectivity and the structure of the pore surfaces are unknown. In this study ^{129}Xe NMR spectroscopy is used to acquire better insight into the structural variations and connectivity of the pores in functionalized mesoporous silica, and the arrangement of these functional molecules in the mesoporous channels as the pore diameter is changed.

In the past twenty years ^{129}Xe NMR has become a popular technique for the characterization of porous solids,[20,21] and several extensive reviews on the subject are available.[22−24] The main advantage of ^{129}Xe NMR is the high sensitivity of the chemical shift to the local environment of the Xe atom. The emphasis in much of the previous work has been placed on developing empirical relationships between chemical shift and pore dimension.[25,26] The limitations and problems associated with such an approach have already been discussed.[26−30] Until recently, applications of ^{129}Xe NMR to pore systems have concentrated mostly on studies of crystalline porous materials such as zeolites. Only a limited number of studies on either amorphous or highly disordered pore systems have been reported. The main obstacle in using ^{129}Xe NMR for structural characterization lies in the fact that the observed chemical shift is dynamically averaged among various xenon environments and therefore cannot be directly related to a specific location. Analysis of all the contributions to the observed shift is usually very complicated.

Application of thermally polarized ^{129}Xe NMR to materials is often hampered by a relatively weak signal due to low concentration of adsorbed xenon and long relaxation times (this is particularly the case for mesoporous silica). An increase in sensitivity of several orders of magnitude can be achieved by using optical pumping techniques for the production of hyperpolarized (HP) xenon.[31] This approach has been used to good advantage in the development of HP xenon imaging for clinical applications, especially lung imaging.[32] For materials applications, recent advances include HP Xe delivery into MAS probes,[33] use of a re-circulating continuous flow system for the recording of Xe spectra of materials in a closed system,[34,35] and chemical shift imaging of porous materials.[36]

In this work the continuous flow hyperpolarized ^{129}Xe NMR technique is used for the first time to characterize pore structures in ordered mesoporous materials. The use of HP Xe has allowed us to perform experiments at very low concentrations of xenon, where the contribution of the Xe−Xe interaction is negligible and the observed ^{129}Xe chemical shift reflects mainly interactions between the xenon atoms and the surface. The utility of this method for characterization of the porosity in nanoporous composite materials is demonstrated.

Experimental Section

Materials. Ordered mesoporous silica (OMS) materials with three different pore sizes 5, 9.3, and 30 nm were synthesized. The OMS sample with pores of 5 nm (OMS-5) was prepared by a standard base-catalyzed technique using cetyltrimethylammonium chloride surfactant.[1,2] OMS-9.3 and OMS-30 samples were prepared via an acid-catalyzed sol−gel procedure using a triblock copolymer, Pluronic P123, and mesitylene as a pore expanding agent.[12,37] Mesoporous silica materials functionalized with alkyl silanes (decyltriethoxysilane, referred to as C_{10}) were prepared from calcined silica which was first suspended in toluene and pretreated with an amount of water corresponding to approximately two monolayers. This suspension was stirred vigorously for 2 h to ensure homogeneous distribution of water throughout the OMS. Then decyltriethoxysilane in an amount corresponding to one monolayer was added and the mixture was refluxed for 6 h. Thus functionalized OMSs (referred to as PNNL materials) were filtered out and washed with toluene and ethanol to remove unreacted silane. The morphology of OMS and PNNL materials was characterized by nitrogen adsorption measurements and TEM.[12]

NMR Measurements. All NMR spectra were measured on a Bruker DSX-400 spectrometer (magnetic field 9.4 T, ^{129}Xe resonance frequency at 110.6 MHz). Two types of ^{129}Xe NMR experiments were performed: (i) with samples sealed in glass tubes with a known amount of preadsorbed xenon (NMR using thermally polarized ^{129}Xe); and (ii) with samples in a continuous flow of hyperpolarized ^{129}Xe.

To prepare a sealed sample, approximately 0.1 g of material was placed into a 5 mm OD glass tube, evacuated at 100 °C for 12−15 h and then loaded with a known amount of xenon gas (Matheson, ^{129}Xe natural isotopic abundance 26.4%). Two sets of sealed samples were studied: low-loaded (LL, 0.5−1 mM of Xe/g) and high-loaded (HL, 2.5−3 mM of Xe/g). Static spectra of sealed samples were recorded with a Morris Instrument Inc. solid-state probe. Magic-Angle Spinning (MAS) spectra were measured at 3.5 kHz using a Bruker BL7 probe with a stretch stator.

The continuous flow (CF) system for production of hyperpolarized (HP) xenon has been described elsewhere.[45] A xenon−helium−nitrogen mixture with a volume composition of 1%−98%−1% was used in all CF HP experiments. The flow rate was monitored with a Vacuum General flow controller (model 80-4) and kept constant in the range of 200−250 scc/min (scc/min − gas flow normalized to standard conditions). In CF HP experiments a flow of HP xenon was delivered directly into the coil region of a modified solid-state probe (Morris Instrument Inc). Variable temperature NMR experiments in the 120−400 K range were also performed with this probe using a Bruker BVT3000 temperature controller. The reported ^{129}Xe NMR chemical shifts were referenced to xenon gas extrapolated to zero pressure.

Results and Discussion

Origin of the ^{129}Xe NMR Chemical Shifts in Porous Materials. First, it is useful to briefly describe the model used in further discussions of the observed chemical shifts. The observed ^{129}Xe NMR signal for adsorbed xenon is the weighted average among various environments sampled by a xenon atom within its characteristic diffusion distance, i.e., $\delta_{obs} = \Sigma_{i=1...n}\, p_i \times \delta_i$, where δ_i is the chemical shift of xenon adsorbed on site i, p_i is the fraction of xenon atoms in site i, and n represents the total number of sites. In porous silica with no paramagnetic impurities and strong adsorption centers, the chemical shift δ_i can be presented as a sum of three principal contributions:[38−41] $\delta_i = \delta_0 + \delta_S + \delta_{Xe-Xe}$. Here δ_0 is the reference shift, which is usually set to 0 ppm, the chemical shift of xenon gas at zero pressure. The term δ_S is the contribution due to the interaction of Xe with the surface. In general, δ_S is characteristic of a given adsorption site and reflects both the chemical composition of

the surface and also the geometry of the xenon environment in that particular site. The chemical shift of adsorbed xenon is known to correlate with the characteristic size of the pore space, and several empirical correlations between the chemical shift and the pore size have been proposed.[25,26,30,40] These correlations are different for different types of porous materials and there is no single equation that would fit any arbitrary porous material. The correlations were tested most comprehensively for zeolites and alumino-phosphate molecular sieves[25,26] (which have voids with a characteristic size between 4 and 12 Å) and for porous silica and silica gels derived from different preparation methods[29,52] (pores between 20 and 400 Å). Although the correlations are not particularly accurate, they can be used to estimate void sizes in systems of a similar nature. Although we discuss only isotropic shifts here, many of the molecular sieves also show Xe chemical shift anisotropy.[24]

The contribution δ_{Xe-Xe} arises from Xe−Xe interactions and is dependent on xenon concentration, shifting the signals to lower field with higher loading. At very low loading, encountered in room-temperature CF experiments, the contribution from the Xe−Xe interactions is rather insignificant. Only for the highly loaded samples and in continuous flow experiments at very low temperatures, where condensation of xenon is possible, does the effect become appreciable. For xenon pressures of several bar the δ_{Xe-Xe} contribution can be of the order of a few ppm. Such downfield shifts of the signals due to increased Xe−Xe interaction in the adsorbed layer at low temperature was previously observed on amorphous silica, alumina, and silica−alumina.[53]

An additional factor that can contribute significantly to the observed ^{129}Xe NMR spectra of porous materials, particularly for samples of poorly defined morphology such as those used in the current work, is the very small size of the particles, which results in an increased exchange between xenon within the pores and on the outer particle surface. The small size of the particles together with the variation in the bulk density arising from differences of powder packing will lead to a variation in line positions, widths, and shapes. Loose packing will usually result in broadening and upfield shifts of the resonance signal. A detailed discussion of the effect of bulk properties on ^{129}Xe NMR of porous materials can be found in ref 54.

Since the Xe chemical shift is dependent on many factors, it is important to realize that no single experiment can provide an unambiguous picture of the pore morphology. Only a combination of experiments can lead to more specific information about the properties and changes in the pore space of the materials due to functionalization. In this work we have tested (a) the variation of the ^{129}Xe chemical shift with xenon loading at ambient temperature, (b) the temperature dependence of the chemical shifts for different samples, and (c) the spin−lattice relaxation time with variation of temperature of adsorbed xenon. The first set of experiments potentially can provide information on the presence of micropores and their connectivity within the mesoporous space. The temperature dependence of the chemical shift is important in understanding the effects of the exchange and for determining associated adsorption parameters. The relaxation time measurements are helpful in understanding the dynamics of the adsorbed xenon and will be discussed in a separate publication.

An important question is whether the ^{129}Xe NMR results obtained in continuous flow experiments can be directly compared with the results from conventional ^{129}Xe NMR experiments, which usually are performed on sealed samples of adsorbent pressurized with xenon gas. Ultimately we need to know how the temperature of the sample is affected by the flow of the gas and if equilibrium is reached under the conditions of the flow experiments. The actual temperature in the region of the NMR coil was tested using the ^{209}Pb NMR signal of solid $Pb(NO_3)_2$,[55] similar to experiments carried out in a closed circuit polarizer.[56] We found that at the relatively low flow rates used in the work presented here (200−250 scc/min), the change in temperature introduced by the flow was well within experimental error of the temperature measurement. Apparently the gas has sufficient time to reach the ambient sample temperature inside the probe. By stopping the flow and recording spectra it is easy to test whether equilibrium conditions are attained. Apart from a dramatic loss of spectral intensity, normally other spectral parameters were not affected. On several occasions we did observe some small changes in the chemical shifts not exceeding 1−1.5 ppm. Considering that the observed lines usually are rather broad and that temperature-induced shifts are significantly larger, these deviations can be considered as unimportant.

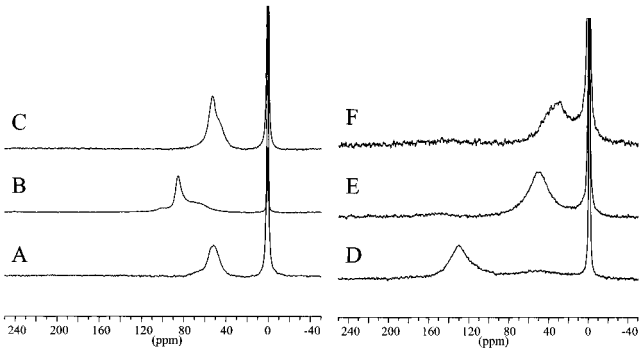

Figure 1. Continuous Flow Hyperpolarized ^{129}Xe NMR spectra of xenon in OMS and PNNL samples: (A) OMS-5, (B) OMS-9.3, (C) OMS-30, (D) PNNL-5, (E) PNNL-9.3, (F) PNNL-30. Differences in the signal-to-noise ratio are due to the differences in adsorption and the number of accumulations.

Room-Temperature ^{129}Xe NMR. Figure 1 shows continuous flow HP ^{129}Xe NMR spectra of the as-prepared all-silica and modified mesoporous materials obtained at 298 K. Measurements at very low partial pressures of xenon in the flowing mixture (1% of total, or ∼10 mbar) preclude contributions from Xe−Xe interactions, and the spectra can be considered as characteristic of the resident framework and the surface. The very low xenon concentration also reduces the rate of exchange between the different adsorption regions, which makes it possible to detect inhomogeneities in the pore space of the materials.

For all of the OMS materials the spectra show several overlapping signals, indicating some variation in the dimensions of the mesoporous channels and, possibly, in the size and aggregation of the primary particles. A particularly complicated spectrum is observed for OMS-9.3, with three partially resolved lines extending over almost 50 ppm (Figure 1B). Together with the fact that N_2 adsorption and TEM data show well ordered and uniform nanoporous channels,[12] such a broad distribution of chemical shifts is likely to be a consequence of inhomogeneity in the structure and porosity of the particles on a micrometer scale. Indeed, scanning electron micrographs (not shown) reveal nonuniform particle distributions. For both 5 and 30 nm OMS samples, the particles are mostly in the micrometer range, while 9.3 nm OMS samples contain substantial amounts of smaller, submicron size particles.

The spectra of the PNNL materials are quite different from those for the nonfunctionalized all-silica materials, and are dominated by two relatively broad signals, one above 130 ppm

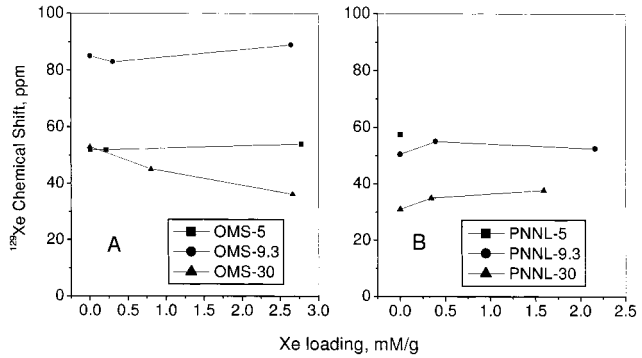

Figure 2. ^{129}Xe NMR chemical shifts as a function of loading for OMS (A) and PNNL (B) samples. The values for the most intense lines in the spectra are shown. For PNNL samples the shifts for the low field lines (above 130 ppm) are not displayed. The solid lines are a visual aid only.

and the other between 30 and 60 ppm. The signal with larger shift is somewhat narrower for PNNL-5, and extremely broad (>8 kHz) for PNNL-9.3 and PNNL-30, with the opposite being true for the signals of smaller chemical shift. The lines with very large shifts for the PNNL samples arise from xenon interaction with the organic phase inside the channels. In some respects the long aliphatic chains "coating" the inside of the channels act as a solvent for xenon, and thus we would expect a shift comparable to that seen in linear saturated hydrocarbon solvents (i.e., 160−190 ppm[40]). When the space inside the channels is mostly blocked, as in PNNL-5, the xenon spends significant time "dissolved" in the organic phase, resulting in a chemical shift in excess of 130 ppm. When, however, considerable free space is present inside the channels,[12] as in PNNL-9.3 or PNNL-30, the exchange between the "dissolved" xenon, xenon on the surface of the organic phase, and free xenon (inside the central void and in the interparticle space) results in a shift of 35−60 ppm.

The reasons for such very broad signals in PNNL samples can be a distribution of adsorption sites for xenon and exchange between the xenon dissolved in the organic phase and void space inside the mesopores and in the external space. The smaller line width for the xenon signal in the organic phase for the PNNL-5 sample (signal at 133 ppm, Figure 1D) results from a reduced exchange rate for this site. It is interesting to note that according to the N_2 adsorption data,[12] the mesopore space of this sample is completely filled by the organic phase. The second line for this sample (at about 57 ppm) likely originates from xenon adsorbed inside the channels, indicating that there must be some nonuniform filling of the mesoporous space with the organic phase. Line broadening in the organic phase for PNNL-9.3 and PNNL-30 samples compared to the PNNL-5 sample indicates a greater exchange contribution.

The ^{129}Xe NMR spectra of sealed OMS and PNNL samples at room temperature (not shown) are similar to those from the CF experiments, although some differences can be seen. For OMS samples these differences appear mainly as variations in line positions and relative signal intensities. In the sealed PNNL samples the signal from xenon dissolved in the organic phase is clearly visible only for the 5 nm PNNL sample. Apparently for the two other PNNL materials the low field signal was not observed because of its breadth, low intensity, and overall low signal-to-noise ratio.

Figure 2 shows the observed ^{129}Xe chemical shift as a function of loading for OMS and PNNL samples (the signals from xenon dissolved in the organic phase are not shown). Counter to expectations, the Xe chemical shift at "zero loading" in OMS materials does not change monotonically with the size of the channels. The shift for the 9.3 nm OMS sample is larger than for the 30 nm sample, and almost twice that for the 5 nm sample (Figure 2A). The magnitude of the chemical shifts deserves special attention. Chemical shifts in the range observed for our OMS samples would normally be expected for much smaller void spaces, similar to those in zeolites.[38−41] If we project the chemical shift vs void size[39,41] dependence generally observed in molecular sieves (by extrapolating to zero xenon pressure) to the size of the channels in our mesoporous materials, the observed shift would be somewhere in the range of 20−0 ppm. The important fact to keep in mind when discussing the chemical shifts of xenon in ordered mesoporous materials prepared with block copolymers is that such materials often contain micropores in the amorphous silica walls[45,57] and on the external surface. The observed ^{129}Xe chemical shifts then represent a dynamic average between Xe sites in the micropores and mesopores and in any interparticle space, leading to the higher observed values. The observation in our materials of such large chemical shifts suggests that they may contain a relatively large concentration of adsorption sites whose sizes are close to that of the xenon atom.

Relatively large chemical shifts of ^{129}Xe adsorbed in mesoporous silicates have been observed recently.[42−44] In one study[42] the large shifts were explained as a result of stronger xenon adsorption present on the microdefects, or the "roughness", of the internal surface of the mesoporous channels. The existence of such "micropores" in the walls of ordered mesoporous materials has been discussed already on the basis of synchrotron X-ray diffraction data.[45] The microporosity in ordered mesoporous materials prepared with block copolymers has been also the subject of a detailed adsorption study.[57]

As an exercise one could try to confirm whether the pore size−chemical shift correlation found for amorphous silica gels[29] would be applicable to all-silica mesoporous materials. The chemical composition of the surface is the same and though the organization of the porous space is quite different, we might expect that the correlation for mesoporous ordered materials may be close to that for amorphous materials. Using the pore diameters from the nitrogen adsorption measurements[12] we calculate shifts of 83, 67, and 35 ppm for the materials containing 5, 9.3, and 30 nm pores, respectively. Only for the 30 nm sample is the observed shift close to that predicted, whereas for the other two samples the observed and predicted shifts disagree by more than 20 ppm.

The changes in the chemical shifts with the loading for both OMS and PNNL samples are not very big and generally do not exceed 10 ppm over the whole range of loading, which is indicative of a weak interaction between xenon and the surface. This has been observed previously for xenon adsorbed in porous[28,29,49,53,54] and nonporous silica.[50,51] For 5 and 9.3 nm OMS samples the shifts increase slightly with increasing loading, as expected for materials where a contribution from Xe−Xe interactions is present. For the OMS-30 sample, however, the changes have the opposite sign (Figure 2). The chemical shift decrease with loading is expected when a small amount of relatively strong adsorption centers is present on the surface.[53] The strong adsorption centers in the case of OMS-30 are likely to be micropores with sizes very close to that of xenon.

The dependence of the chemical shift on xenon loading for the PNNL samples is noticeably different from the corresponding OMS samples (Figure 2B). This is evidently a result of interference by the hydrocarbon chains. It is interesting to note that the observed "zero loading" shifts for the 9.3 and 30 nm

PNNL samples are very close to predictions from the empirical chemical shift−pore size relationship for amorphous silicas.[29] Functionalization of the OMS-9.3 sample produced an almost 30 ppm upfield shift. The disappearance of the "abnormalities" in absolute values of the chemical shift, which were seen for the OMS samples, is likely a result of blocking most of the surface with the bound organic chains. Similar high field ^{129}Xe shifts during coadsorption of water and hydrocarbon have been observed for MCM-41 and were explained in terms of a screening of the roughness of the surface.[42] For PNNL-9.3 the change of the shift with loading is considerably smaller than for the original all-silica material, perhaps indicating a screening effect by the organic phase on the interaction of xenon with the silicate walls. In PNNL-30, however, the chemical shift dependence is opposite in sign to that in OMS-30. The explanation of such a discrepancy in the variation of the ^{129}Xe chemical shift on loading for PNNL-9.3 and PNNL-30 samples probably lies in differences in the assembly of the organic phase for channels of different diameters.

Observed line width variations in measured spectra require a special consideration. As already mentioned, all samples display quite broad signals, ranging between 1 and 3 kHz for OMS, and even in excess of 8 kHz in the PNNL samples. The framework of neither material has considerable concentration of nuclei with large magnetic moments, so nuclear dipole−dipole interactions cannot be responsible for such broadening. Proton decoupling and MAS experiments (not shown) do not produce any significant narrowing of the lines. Since the exchange between xenon atoms in different environments inside a single grain of material is usually fast on the NMR time scale, the distribution of grain sizes most likely contributes to the relatively broad and asymmetric line-shape. The effect of particle size of porous materials on ^{129}Xe NMR spectra has been discussed previously.[29,54] This is obviously the case for an OMS-9.3 sample, where in addition to the unexpectedly large chemical shifts (Figure 1B) also the particularly broad and asymmetric line-shape comprised of a relatively narrow signal that overlaps with a very broad signal is observed. The broad particle size distribution for OMS-9.3, which is very different from that for OMS-5 and OMS-30, may give rise to these complex chemical shifts and line-shapes. The higher chemical shift for the narrow signal may be due to a fast exchange between microporous and mesoporous regions within the same grain of a particle, while the lower chemical shift for the broader signals may result from slow exchange between the channels and the interparticle gas phase.

For some of the samples, there is also a small contribution to the observed line shape from chemical shift anisotropy. This contribution is apparently very small since the position of the signals does not change more than 1−3 ppm downfield under MAS. Spinning the samples at high speed, however, also compresses the samples, which produces an additional permanent shift of the observed signal (i.e., the shift remains even for static samples after they were spun at 3−4 kHz for a few minutes). The latter observation further signifies a contribution of the bulk properties of the materials to the observed spectra.

From all of the observations it is evident that (a) all the samples have regions of different porosities, and these regions are closely connected; and (b) it appears that the mesoporous regions are not homogeneous. For OMS samples, at least two overlapping lines appear in the spectra. Although the difference in shifts between the lines is not significant, the pore space distribution is evident. A reasonable model to explain these observations would be fast exchange between meso- and micropores within one adsorption region, with somewhat reduced exchange between the different mesoporous regions. The micropore sites must be present in the same phase as the mesopore sites, i.e., within the same grain, and likely are present as pockets along the mesopore channel walls. The presence of different mesopore regions found with ^{129}Xe NMR does not necessarily mean that there is a variation in the channel sizes, as dispersion in the chemical shift is also expected when there is a distribution in the size of individual grains.

Variable-Temperature ^{129}Xe NMR Spectra. Variations in ^{129}Xe NMR spectra with temperature can be very sensitive to the dynamics of adsorbed xenon and subsequently to the morphology of the pore space.[28,29,44,53,54] By performing variable-temperature (VT) ^{129}Xe NMR, it should be possible to differentiate xenon in the micropore and mesopore regions and obtain heats of adsorption. We measured VT static ^{129}Xe spectra using continuous flow (CF) HP xenon for all of the materials. The use of HP Xe removed the limitation of long acquisition times required for thermally polarized Xe because of the associated low sensitivity and long relaxation time. VT spectra measured using thermally polarized Xe for the highly loaded sealed samples were found to be essentially the same as for the CF experiments.

The spectra obtained with CF HP xenon are shown in Figures 3 and 4 for OMS and PNNL, respectively. The intense line at 0 ppm in all of these spectra is from xenon in the gas phase. All lines at lower field originate from adsorbed xenon. Spectra in both figures show shifts to lower field with decreasing temperature.

OMS Samples. The variable temperature spectra of OMS-5 and OMS-30 are somewhat similar. At 373 K the spectra display a broad unresolved signal centered at 25 ppm for OMS-5, and two partially resolved signals with similar chemical shifts at 15 and 18 ppm for OMS-30 (Figures 3A and 3C). At approximately 200 K the lines merge. The remaining signal continues to shift downfield at a slower rate than that at higher temperatures and is almost temperature invariant below 180 K. At 163 K, partially resolved signals are observed centered at ∼110 ppm for OMS-5, while a narrow signal appears at 142 ppm for OMS-30. It is interesting to note that for these OMS samples the limiting shifts of signals at the lowest temperatures are higher for the samples with larger channels.

As discussed in the previous section, the behavior of the OMS-9.3 sample is somewhat different from the other two samples (see Figure 3B). Between 273 and 313 K the spectra display three unresolved signals which at lower temperatures collapse into a single line (138 ppm at 163 K), and separate into two well-resolved lines at higher temperature (30 and 58 ppm at 373 K). However, for the 5 and 30 nm samples at elevated temperatures all the lines are shifted to high field and reach the 20−30 ppm region at 373 K.

These VT observations demonstrate that in all of the OMS samples xenon is in fast exchange between at least two distinct adsorption regions, which, from the VT behavior of the shift, can be assigned to regions of micro- and mesoporosity. At lower temperature, xenon principally occupies the micropore space while at higher temperatures, it samples the mesopore region. Each region likely is not homogeneous, which is seen in the asymmetry and broadening of the signals at the lowest and the highest temperatures. We can conclude, therefore, that although N_2 adsorption and TEM results show ordered nanoporous channels,[12] the ^{129}Xe NMR spectra in this study reveal nonuniform porosity and an irregular pore structure.

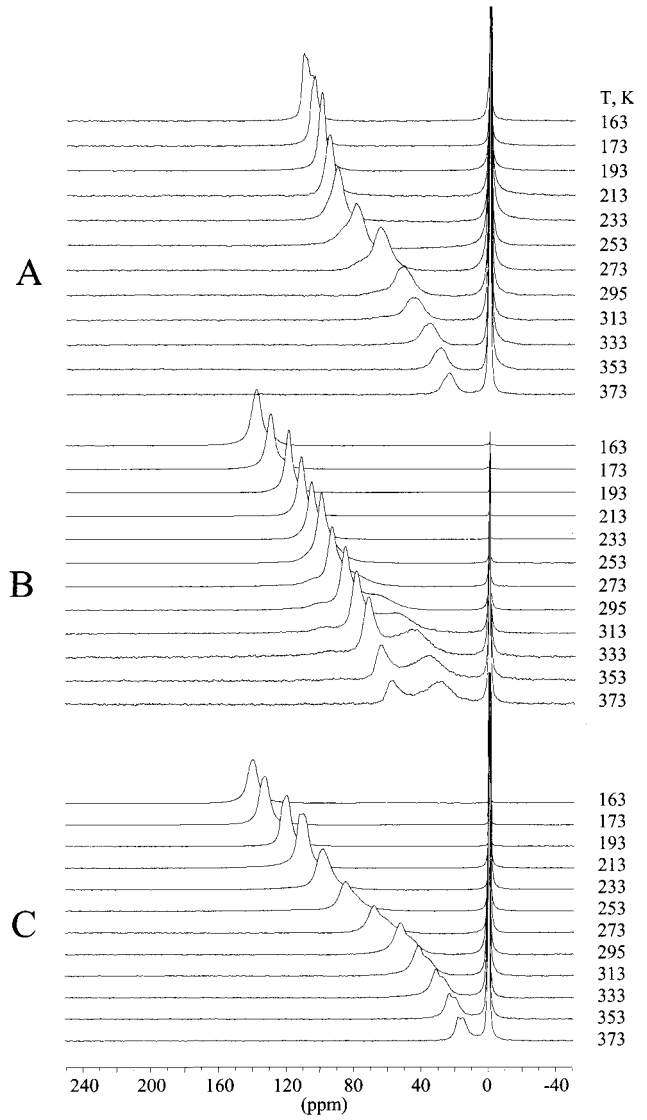

Figure 3. Variable temperature CF HP ^{129}Xe NMR: (A) OMS-5, (B) OMS-9.3, (C) OMS-30.

PNNL Samples. The temperature dependencies of the CF HP spectra for the PNNL samples shown in Figure 4 are somewhat different from those for the OMSs and generally are more complicated. The spectra of PNNL-9.3 and PNNL-30 samples look very similar. The PNNL-5 sample shows a more complex pattern. First, for all three samples the xenon signals do not collapse when the temperature goes down and two signals are observed even at the lowest temperature. For the PNNL-9.3 and PNNL-30 the spectra at 163 K consist of a very broad line at ~198 ppm and a narrower line at ~132−133 ppm. The latter line has a chemical shift close to that observed in unmodified OMSs and is assigned to xenon on the silica surface (δ_s). The shift of the other line is close to that observed for xenon in polymers and in solutions of hydrocarbons with long hydrocarbon chains.[23,24,48,50] Similarly the PNNL-5 sample shows two unresolved signals at ~189 and ~166 ppm. For all three samples, as temperature increases the lines shift to higher field. For PNNL-9.3 and PNNL-30 the signals move very close to each other, but do not coalesce, at around 213 K. Above this temperature the separation between the signals increases again. The lower field signal becomes almost temperature independent and broadens steadily until it completely disappears at 300 K. The second signal shifts to higher field and at 373 K reaches 22 and 14 ppm for PNNL-9.3 and PNNL-30, respectively. Here,

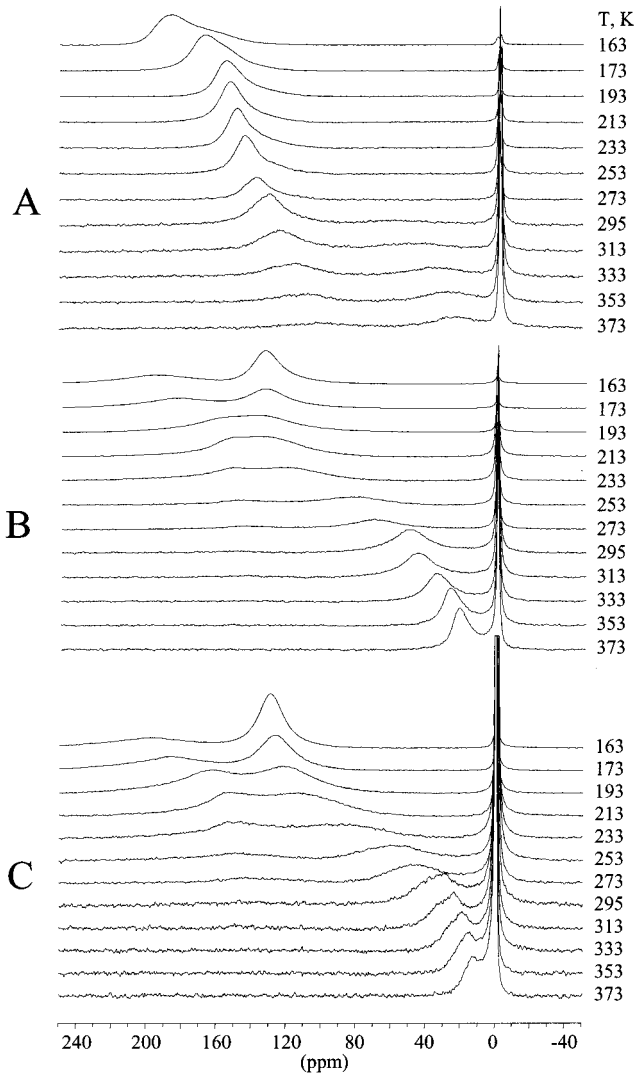

Figure 4. Variable temperature CF HP ^{129}Xe NMR spectra: (A) PNNL-5, (B) PNNL-9.3, (C) OMS-30.

the chemical shift trend for PNNL-9.3 correlates with the size of the pore, indicating that the modification of the surface of OMS-9.3 removes most of the surface defects. In the case of PNNL-5, however, the signals collapse into a single line near 157 ppm at around 190 K. The line moves continuously upfield with the increasing temperature and broadens gradually until it almost disappears close to 103 ppm at 373 K. An additional line at 61 ppm emerges for this sample above 280 K, and slowly shifts to 23 ppm at 373 K. Both signals at 23 and 103 ppm at 373 K for PNNL-5 are less intense than those for PNNL-9.3 and PNNL-30, indicating most mesopore channels are blocked by the bound molecules, which is in agreement with our previous findings.[12]

Similar to the OMS materials, these observations can be understood in terms of the coexistence of two regions of porosity with fast xenon exchange between them. In the case of the PNNL samples, however, the situation is complicated by the presence of the hydrocarbon chains inside the mesopores. The effect of these hydrocarbon chains is 2-fold. First, they partially block xenon from access to the silica surface. Second, xenon interacts with the hydrocarbon chains, forming a kind of "solution" in the organic phase. This interaction results in a very high Xe chemical shift exceeding 200 ppm.

For materials with larger channels (PNNL-9.3 and PNNL-30), some regions of bare silica surface are still accessible, which

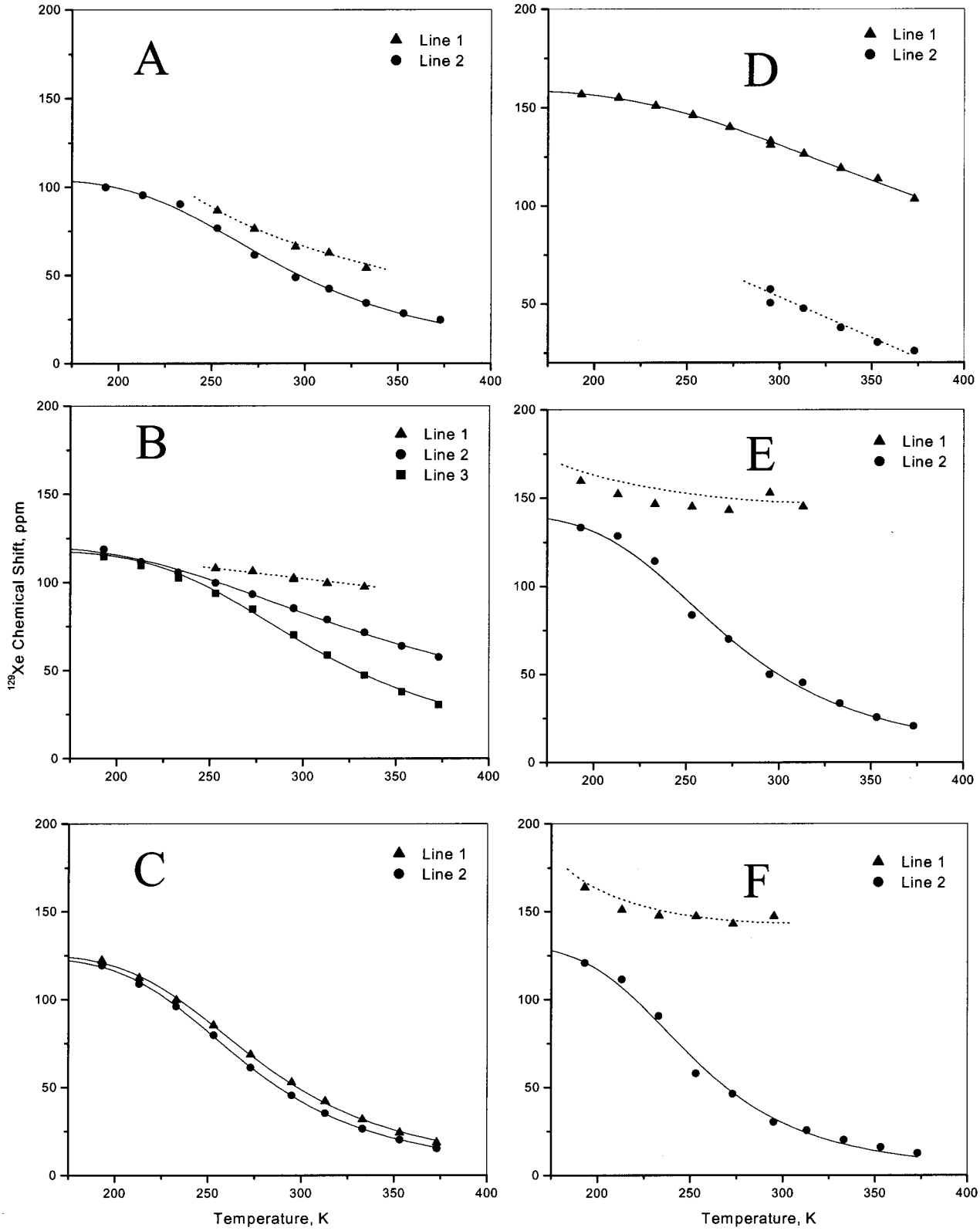

Figure 5. Variation of the measured ^{129}Xe chemical shift with the temperature in CF HP Xe experiments for OMS and PNNL samples. Points are experimental data, solid lines are fits using eq 1. The dotted lines in A, B, D, E, and F, shown with the points for signals which do not appear over the full temperature range, are not fits but a visual aid only.

is evident from the observation of a signal at around 130 ppm in the low temperature spectra. The increased visibility of the bare silica regions at low temperature indicates the involvement of thermally activated processes. A possible explanation is that the fast reorientation of the surface-bound hydrocarbon chains at higher temperatures effectively prevents xenon from reaching the surface and reduces its interaction with the bare silica. At the lower temperatures the motion of the chains is significantly reduced, and the surface of bare silica is not as effectively covered. One must also consider that at reduced temperature the hydrocarbon chains freeze into a more dense conformation, thus squeezing xenon out of solution much as what happens when a liquid containing xenon is frozen. Overall, this results in an increased contribution from the silica regions to the

observed signal. For PNNL-5, however, the blockage of the channel pore space is complete, and even at low temperatures xenon hardly reaches the surface of the channels.

In general, variations in the spectra for the sealed samples with the temperature (not shown here) are very similar to those observed in CF experiments, although some differences were observed, particularly for the samples with modified surfaces. First, for all the samples, the range of changes in the chemical shift with temperature is somewhat larger in experiments with sealed samples. Though at higher temperatures the shifts are very similar, the low temperature shifts when the signals start to level off are consistently higher by approximately 20−25 ppm. These higher shifts can be attributed to stronger Xe−Xe interactions in the sealed samples because of the higher concentration of xenon on the surface. The very low pressure of xenon in the CF experiments will produce a very dilute adsorption layer with a very weak contribution of Xe−Xe interactions to the shift. Only at temperatures below 180 K when the condensation of xenon becomes significant does the contribution of Xe−Xe in the CF spectra become significant. This can be seen in a steep (∼1 ppm/K) increase in the chemical shift as the temperature drops below 180 K. Second, in contrast to the sealed samples, the CF spectra for all samples with modified surface space clearly demonstrate a fairly broad separated signal with a shift above 140 ppm at temperatures below 273 K. This signal remains unchanged down to about 200 K after which it shifts gradually above 200 ppm. The signal is assigned to xenon dissolved in the organic phase and in slow exchange with the gas phase. The fact that this signal is not observed in the sealed samples can be explained by (a) accumulation of xenon in the organic phase under CF, and (b) poor visibility of this line in the spectra of sealed samples because of severe broadening. The latter is supported by the observation in the spectra of PNNL-9.3-HL, where below 200 K a very broad weak line with a shift near 220 ppm can be seen.

The temperature dependencies of the chemical shift in CF HP ^{129}Xe NMR experiments are summarized in Figure 5. Assuming only a weak adsorption of xenon which can be described by Henry's law, one can extract some quantitative information on the Xe adsorption.[29] In the fast exchange approximation the temperature dependence of the observed chemical shift δ for cylindrical pores can be expressed as:[29]

$$\delta = \delta_s\left(1 + \frac{D}{4K_0RT^{1/2}\exp\left(\frac{\Delta H_{ads}}{RT}\right)}\right)^{-1} \qquad (1)$$

In this equation K_0 is the pre-exponent in the Henry equation, D is the channel diameter, R is the universal gas constant, ΔH_{ads} is the heat of adsorption, and δ_s is the chemical shift of xenon in contact with the surface. The xenon adsorption in the CF experiments does not exceed 1 mmol/g even for the lowest temperatures, which represents a surface coverage of about 100 m^2/g or 0.1 to 0.2 of a monolayer of xenon.[12] Under these conditions δ_s can be approximated by the chemical shift observed at the lowest temperature before xenon starts to condense (∼180 K in CF experiments). Figure 5 shows fits using eq 1 of the VT dependencies of the chemical shift for OMS and PNNL samples in CF experiments. Parameters obtained from the fits are summarized in Table 1. Similar dependencies were obtained for sealed samples with high xenon loading. However, because of the increased contribution from Xe−Xe interactions in the sealed samples, fitting their chemical shift dependence is expected to increase the uncertainty in the value of ΔH_{ads} (underestimated) and for this reason they are not reported.

TABLE 1: Fitting Parameters for the Variable Temperature^{129}Xe Chemical Shifts in OMS and PNNL Samples (The fitting was done for two signals if they were sufficiently separated.)

	D,	δ_s, ppm	ΔH, kJ/mol	K_o, Torr^{-1} m^{-2}	K(298), Torr^{-1} m^{-2}
OMS-5	5	107	16.2 ± 0.6	0.54×10^{11}	0.38×10^{14}
OMS-9.3	9.3	121	13.3 ± 0.6	7.7×10^{11}	1.7×10^{14}
	9.3	118	18.3 ± 0.6	6.6×10^{11}	1.0×10^{14}
OMS-30	30	126	18.3 ± 0.4	1.0×10^{11}	1.6×10^{14}
	30	124	18.7 ± 0.3	0.72×10^{11}	1.4×10^{14}
PNNL-5[a]	N/A[b]	160[c]	N/A	N/A	N/A
PNNL-9.3	5.6[b]	141	17.8 ± 1	0.19×10^{11}	0.25×10^{14}
PNNL-30	17.5[b]	151	18.5 ± 1.1	0.24×10^{11}	0.43×10^{14}

[a] It is unlikely that the fast exchange model is correct in the case of PNNL-5, and fitting was not done for this case. [b] The effective diameters of the channels in PNNL samples are taken from ref 12. [c] Extrapolated value for the signal of xenon dissolved in the organic phase.

The values found for ΔH_{ads} fall between 13 and 18 kJ/mol indicating that in all cases only physical adsorption takes place. Strictly speaking the Henry constants obtained by this method should be considered only as rough estimates because of the assumption of a very narrow pore size distribution. All the constants, however, have reasonable values and compare rather favorably with values obtained from adsorption measurements. The Henry constants obtained for OMS samples from adsorption measurements at 298 K are 9.2×10^{13}, 5.2×10^{13}, and 5.6×10^{13} Torr^{-1} m^{-2} for OMS-5, OMS-9.3, and OMS-30, respectively. Some over-estimates in the constants found from the NMR data are not unreasonable in view of all the simplifications that have been made. Also note that the analysis of NMR data is based on a particular pore size, whereas the constants from the adsorption measurements are the average for the whole sample including external surface, amorphous regions, impurities, etc. The relatively high preexponential factor K_o of the Henry constants found for the low field signal in the OMS-9.3 sample can probably be associated with the higher fraction of microporous space or more surface defects as discussed previously in this paper.

Conclusions

We have performed extensive NMR chemical shift measurements of ^{129}Xe adsorbed in mesoporous materials with different porosities and surface functionalization. For the first time we demonstrate the application of continuous flow hyperpolarized ^{129}Xe techniques to studies of pore structure and heterogeneity in ordered mesoporous materials. The use of HP ^{129}Xe allowed us to work with very low concentrations of xenon, where the observed ^{129}Xe chemical shift is principally associated with interactions between the xenon atoms and the surface. Variable temperature measurements provided information regarding Xe adsorption parameters and their changes due to modification of the mesoporous spaces. Although N_2 adsorption and TEM show ordered nanoporous channels, ^{129}Xe NMR reveals a nonuniform porosity and irregular pore structure.

Acknowledgment. This work was partly supported by the Division of Materials Sciences and Engineering, Office of Basic Energy Sciences, U.S. Department of Energy (USDOE). Pacific Northwest National Laboratory is a multiprogram national laboratory operated for the USDOE by Battelle Memorial Institute under Contract DE-AC06-76RL0 1830.

References and Notes

(1) Kresge, C. T.; Leonowicz, M. E.; Roth, W. J.; Vartuli, J. C.; Beck, J. S. *Nature* **1992**, *359*, 710.

(2) Beck, J. S.; Vartuli, J. C.; Roth, W. J.; Leonowicz, M. E.; Kresge, C. T.; Schmitt, K. D.; Chu, C. T.-W.; Olson, D. H.; Sheppard, E. W.; McCullen, S. B.; Higgins, J. B.; Schlenker, J. L. *J. Am. Chem. Soc.* **1992**, *114*, 10834.

(3) (a) Pelrine, B. P.; Schmitt, K. D.; Vartuli, J. C. U.S. Patent 5,-105,051, 1992; (b) Beck, J. S.; Socha, R. F.; Shihabi, D. S.; Vartuli, J. C. U.S. Patent 5,143,707, 1992; (c) Le, Q. N.; Thompson, R. T.; Yokomizo, G. H. U.S. Patent 5,134,242, 1992; (d) Le, Q. N.; Thompson, R. T. U.S. Patent 5,232,580, 1993; (e) Le, Q. N. U.S. Patent 5,118,894, 1992.

(4) Sayari, A. *Chem. Mater.* **1996**, *8*, 1840.

(5) Behrens, P.; Stucky, G. D. *Angew. Chem., Int. Ed. Engl.* **1993**, *32*, 696.

(6) (a) Vandry, F.; Khodabandeh, S.; Davis, M. E. *Chem. Mater.* **1996**, *8*, 1451. (b) Bagshaw, B. A.; Pinnavia, T. J. *Angew. Chem., Int. Ed. Engl.* **1996**, *3* (5), 1102. (c) Knowles, J. A.; Hudson, M. J. *J. Chem. Soc., Chem. Commun*. **1995**, 2083. (d) Schmidt, R.; Akporiaye, D.; Stöcker, M.; Ellestad, O. H. *J. Chem. Soc., Chem. Commun.* **1994**, 1493. (e) Antonelli, D. M.; Ying, J. Y. *Chem. Mater.* **1996**, *8*, 874. (f) Antonelli, D. M.; Ying, J. Y. *Angew. Chem., Int. Ed. Engl.* **1995**, *34*, 2014.

(7) Tian, Z.-R.; Tong, W.; Wang, J.-Y.; Duan, N.-G.; Krishnan, V. V.; Suib, S. L. *Science* **1997**, *276*, 926.

(8) Zhao, D.; Yang, P.; Huo, Q.; Chmelka, B. F.; Stucky, G. D. *Curr. Opin. Solid Mater.* **1998**, *3*, 111.

(9) (a) Mercier, L.; Pinnavaia, T. J. *Adv. Mater.* **1997**, *9*, 500. (b) Mercier, L.; Pinnavaia, T. J. *Environ. Sci. Technol.* **1998**, *32*, 2749.

(10) (a) Feng, X.; Fryxell, G. E.; Wang, L.-Q.; Kim, A. Y.; Kemner, K.; Liu, J. *Science* **1997**, *276*, 923. (b) Liu, J.; Feng, X.; Fryxell, G. E.; Wang, L.-Q.; Kim, A. Y.; Gong, M. *Adv. Mater.* **1998**, *10*, 161.

(11) Fryxell, G. E.; Liu, J.; Hauser, T. A.; Nie, Z.; Ferris, K. F. *Chem. Mater.* **1999**, *11*, 2148.

(12) Liu, J.; Shin, Y.; Nie, Z.; Chang, J. H.; Wang, L.-Q.; Fryxell, G. E.; Samuels, W. D.; Exarhos, G. J. *J. Phys. Chem. A* **2000**, *104*, 8328.

(13) Feng, X.; Rao, L.; Mohs, T. R.; Xu, J.; Xia, Y.; Fryxell, G. E.; Liu, J.; Raymond, K. N. Self-assembled Monolayers on Mesoporous Silica, a Super Sponge for Actinides. *Ceram. Trans.* (*Environmental Issues and Waste Management Technologies IV*) **1999**, *93*, 35−42.

(14) Moller, K.; Bein, T. *Chem. Mater.* **1998**, *10*, 2950.

(15) Cauvel, D.; Renard, G.; Brunel, D. *J. Org. Chem.* **1997**, *62*, 749.

(16) Burkett, S. L.; Simms, S. D.; Mann, S. *J. Chem. Soc., Chem. Commun.* **1996**, 1367.

(17) Lim, M. H.; Blanford, C. F.; Stein, A. *Chem. Mater.* **1998**, *10*, 467.

(18) (a) Whitesides, G. M. *Sci. Amer.* **1995**, *273*, 146. (b) Ulman, A. *Chem. Rev.* **1996**, *96*, 1533.

(19) (a)Wang, L.-Q.; Exarhos, G. J.; Liu, J. *Adv. Mater.* **1999**, *11*, 1331. (b) Wang, L.-Q.; Liu, J.; Exarhos, G. J.; Bunker, B. C. *Langmuir* **1996**, *12*, 2663.

(20) Ito, T.; Fraissard, J. *J. Chem. Phys.* **1982**, *76*, 5225.

(21) Ripmeester, J. A. *J. Am. Chem. Soc.* **1982**, *104*, 289.

(22) Barrie, P. J.; Klinowski, J. *Prog. Nucl. Magn. Reson. Spectrosc.* **1992**, *24*, 91.

(23) Raftery, D.; Chmelka B. F. *Nucl. Magn. Reson. Basic Princ. Prog.* **1994**, *30*, 111.

(24) Ratcliffe, C. I. *Annu. Rep. Nucl. Magn. Reson. Spectrosc.* **1998**, *36*, 124.

(25) (a) Fraissard, J.; Ito, T. *Zeolites* **1988**, *8*, 350, (b) Demarquay, J.; Fraissard, J. *Chem. Phys. Lett.* **1987**, *136*, 314.

(26) Chen, Q.; Springuel-Huet, M. A.; Fraissard, J. *Stud. Surf. Sci. Catal.* **1991**, *65*, 219.

(27) Annen, M. J.; Davis, M. E.; Hanson, B. E. *Catal. Lett.* **1990**, *6*, 331.

(28) Ripmeester, J. A.; Ratcliffe, C. I. *J. Phys. Chem.* **1990**, *94*, 7652.

(29) Terskikh, V.; Mudrakovski, I.; Mastikhin, V. *J. Chem. Soc., Faraday Trans.* **1993**, *89*, 4239.

(30) (a) Jameson, C. J.; Jameson, K. A.; Lim, H.-M.; Baello, B. I. *J. Chem. Phys.* **1994**, *100*, 5977; (b) Jameson, C. J.; Jameson, A. K.; Gerald, R. E., II.; Lim, H.-M. *J. Chem. Phys.* **1995**, *103*, 8811. (c) Jameson, C. J.; Jameson, A. K.; Lim, H.-M. *J. Chem. Phys*. **1996**, *104*, 1709.

(31) (a) Grover, B. C. *Phys. Rev. Lett.* **1978**, *40*, 391. (b) Happer, W.; Miron, E.; Schaefer, S.; Schreiber, D.; van Wingaarden, W. A.; Zeng, X. *Phys. Rev. A* **1984**, *29*, 3092.

(32) (a) Albert, M. S.; Cates, G. D.; Driehuys, B.; Happer, W.; Saam, B.; Springer, C. S.; Wishnia, A. *Nature* **1994**, *370*, 199. (b) Mugler, J., III.; Driehuys, B.; Brookeman, J.; Cates, G. D.; Berr, S.; Bryant, R. G.; Daniel, T. M.; de Lange, E.; Downs, J. H., III.; Erickson, C. J.; Happer, W.; Hinton, D. P.; Kassel, N. F.; Maier, T.; Phillips, C. D.; Saam, B.; Sauer, K. L.; Wagshul, M. E. *Magn. Res. Med.* **1997**, *37*, 809.

(33) Raftery, D.; MacNamara, E.; Fisher, G.; Rice, C. V.; Smith, J. *J. Am. Chem. Soc.* **1997**, *119*, 8746.

(34) Haake, M.; Pines, A.; Reimer, J. A.; Seydoux, R. *J. Am. Chem. Soc.* **1997**, *119*, 11711.

(35) (a) Seydoux, R.; Pines, A.; Haake, M.; Reimer, J. A. *J. Phys. Chem. B* **1999**, *103*, 4629. (b) Brunner, E.; Haake, M.; Kaiser, L.; Pines, A.; Reimer, J. A. *J. Magn. Reson*. **1999**, *138*, 155.

(36) (a) Moudrakovski, I. L.; Lang, S.; Ratcliffe, C. I.; Simard, B.; Santyr, G.; Ripmeester. J. A. *J. Magn. Reson*. **2000**, *144*, 372. (b) Kaiser, L.; Meersmann, T.; Logan, J.; Pines, A. *Proc. Natl. Acad. Sci.* **2000**, *97*, 2414.

(37) (a) Chen, C. Y.; Li, H. X.; Davis, M. E. *Microporous Mater.* **1993**, *2*, 17. (b) Chen, C. Y.; Burkett, S. L.; Li, H. X.; Davis, M. E. *Microporous Mater.* **1993**, *2*, 27.

(38) Bonardet, J. L.; Fraissard, J.; Gedeon, A.; Springuel-Huet, M. A. *Catal. Rev. Sci. Eng.* **1999**, *41*, 115.

(39) Chen, Q. J.; Springuel-Huet, M. A.; Fraissard, J. *Studies Surf. Sci. Catal.* **1991**, *65*, 219.

(40) Springuel-Huet, M. A.; Bonardet, J. L.; Gedeon, A.; Fraissard, J. *Magn. Res. Chem.* **1999**, *37*, S1.

(41) Springuel-Huet, M. A.; Bonardet, J. L.; Fraissard, J. *Appl. Magn. Res.* **1995**, *8*, 427.

(42) Springuel-Huet, M. A.; Sun, K.; Fraissard, J. *Microporous Mesoporous Mater.* **1999**, *33*, 89.

(43) Pietrass, T.; Kneller, J. M.; Assink, R. A.; Anderson, M. T. *J. Phys. Chem. B* **1999**, *103*, 8837.

(44) Jong, S.-J.; Wu, J.-F.; Pradhan, A.; Lin, H.-P.; Mou, C.-Y.; Liu, S.-B. *Stud. Surf. Sci. Catal.* **1998**, *117*, 543.

(45) Edler, K. J.; Reynolds, P. A.; White, J. W.; Cookson, D. *J. Chem. Soc., Faraday Trans.* **1997**, *93*, 199.

(46) Stengle, T. R.; Reo, N. V.; Williamson, K. L. *J. Phys. Chem*. **1981**, *85*, 3772.

(47) Hunt, E. R.; Carr, H. Y. *Phys. Rev.* **1963**, *130*, 2302.

(48) Jokisaari, J. *Prog. Nucl. Magn. Res. Spectrosc*. **1994**, *26*, 1.

(49) Springuel-Huet, M. A.; Fraissard, J.; Schmidt, R.; Stoker, M.; Conner, W. C. C. *Pub. Royal Soc. Chem.* **1997**, 452.

(50) Ripmeester, J. A.; Ratcliffe, C. I. *J. Phys. Chem.* **1990**, *94*, 7652.

(51) Conner, W. C.; Weist, E. L.; Ito, T.; Fraissard, J. *J. Phys. Chem.* **1989**, *93*, 4138.

(52) Julbe, A.; De Menorval, L. C.; Balzer, C.; David, P.; Palmeri, J.; Guizard, C. J. *Porous Mater.* **1999**, *6*, 41.

(53) Cheung, T. T. P. *J. Chem. Phys.* **1989**, *93*, 7549.

(54) Ripmeester, J. A.; Ratcliffe, C. I. *Anal. Chim. Acta* **1993**, *283*, 1103.

(55) Bielecki, A.; Burum, D. P. *J. Magn. Reson. A* **1995**, *116*, 215.

(56) Kneller, J. M.; Soto, R. J.; Surber, S. E.; Colomer, J.-F.; Fonseca, A.; Nagy, J. B.; Pietrass, T. *J. Magn. Reson*. **2000**, *147*, 261.

(57) Galarneau, A.; Cambon, H.; Di Renzo, F.; Fajula, F. *Langmuir* **2001**, *17*, 8328.